Band offset determination of atomic-layer-deposited Al2O3 and HfO2 on InP by internal photoemission and spectroscopic ellipsometry

K. Xu, H. Sio, O. A. Kirillov, L. Dong, M. Xu et al.

Citation: J. Appl. Phys. **113**, 024504 (2013); doi: 10.1063/1.4774038
View online: http://dx.doi.org/10.1063/1.4774038
View Table of Contents: http://jap.aip.org/resource/1/JAPIAU/v113/i2
Published by the American Institute of Physics.

Band offset determination of atomic-layer-deposited Al_2O_3 and HfO_2 on InP by internal photoemission and spectroscopic ellipsometry

K. Xu,[1,2] H. Sio,[1] O. A. Kirillov,[1] L. Dong,[2] M. Xu,[2] P. D. Ye,[2] D. Gundlach,[1] and N. V. Nguyen[1,a)]
[1]*Semiconductor and Dimensional Metrology Division, National Institute of Standards and Technology, Gaithersburg, Maryland 20899, USA*
[2]*Purdue University, West Lafayette, Indiana 47907, USA*

(Received 2 July 2012; accepted 17 December 2012; published online 9 January 2013)

Band offsets at the interfaces of n- and p-type InP ((100) and (111)A) and atomic-layer-deposited (ALD) Al_2O_3 were measured with internal photoemission and spectroscopic ellipsometry. Similarly, the band offsets at the interface of semi-insulating InP (100) and ALD HfO_2 were also determined. The barrier between the top of InP valence band (VB) and the bottom of Al_2O_3 conduction band (CB) is found to be 3.44 eV for p-type material and 3.53 eV for n-type. The photoemission thresholds are found to be sensitive to the annealing conditions, and blue shifts are observed after annealing. The offsets from InP valence band to the HfO_2 conduction band for the HfO_2/InP stack are found to be 3.89 eV, and we observed an increase of 60 meV if the InP surface is passivated. © *2013 American Institute of Physics*. [http://dx.doi.org/10.1063/1.4774038]

I. INTRODUCTION

New materials and manufacturing technologies are in demand as further scaling down of complementary metal-oxide-semiconductor (CMOS) integrated circuits (ICs) is reaching its physical limits. Atomic-layer-deposited (ALD) high-κ on III-V has attracted much attention due to their high electron mobility and saturation velocity.[1] The interface quality of high-κ dielectric on III-V substrates remains to be a major challenge, although significant progress has been made in the past years.[2–6] Among high-mobility III-V compound semiconductor materials, InP is more forgiving than GaAs in the aspect of Fermi-level pinning and has a higher saturation velocity of 2×10^7 cm/s.[2] InP metal-oxide-semiconductor field-effect transistor (MOSFET) devices with ALD gate dielectric exhibiting high drain current have been previously reported.[2–6] To determine the magnitude of improvement in device performance, the knowledge of accurate band offsets between InP and gate oxide is required, as sufficiently high energy barrier at the oxide interface is of critical importance.[7] The electron band alignment between InP (100) and ALD Al_2O_3 with various passivation methods was measured using internal photoemission (IPE) by Chou *et al.*,[8] and the barrier height between the valence band (VB) top of InP to the conduction band (CB) top of alumina was reported to be 4.05 ± 0.10 eV. An interlayer was also observed between the InP substrate and the oxide.[8] In this article, we provide a broader picture by examining different crystalline orientations of InP [(100) and (111)A, the In-terminated polar surface] and the effects of post-deposition annealing (PDA) for an Al/Al_2O_3/InP MOS stack, and further investigate the band alignment of an Al/HfO_2/InP stack, by means of spectroscopic ellipsometry (SE) and IPE.

II. EXPERIMENTS AND DATA ANALYSIS

MOS structures consisting of Al metal gate, Al_2O_3 insulator, and n- or p-type InP were used. An 8 nm ALD Al_2O_3 was grown after InP surface degreasing, removal of native oxide by a 30 s buffered-oxide-etch (BOE), and a 10 min $(NH_4)_2$ S-based passivation, all performed at room temperature. Post-deposition annealing was performed at 500 °C for 30 s in N_2 ambient. An optically semi-transparent Al metal gate of 12 nm thickness was defined by photolithography and a lift-off process after being thermally evaporated on top of the ALD oxide.

For the Al/HfO_2/InP stack, a 10 nm HfO_2 layer was grown on top of semi-insulating InP substrate after BOE and $(NH_4)_2$ S-based passivation. Semi-transparent Al gate of 12 nm is then thermally evaporated and patterned. Process conditions are the same as the Al/Al_2O_3/InP stack mentioned earlier. To avoid any major voltage drop at the back contact that may interfere with our measurements, Ni/Ge/Au was deposited to the backside of the InP substrate by thermal evaporation. The sample was then annealed at 400 °C for 30 s in a N_2 ambient to form an ohmic contact.

Vacuum ultraviolet spectroscopic ellipsometry (VUV-SE) is used to determine the optical bandgap of Al_2O_3 and HfO_2 and to verify the origin of special features present in the IPE spectra, which will be discussed later in detail. The bandgap, E_g, for an amorphous material is determined from the energy dependence of its absorption coefficient, $\alpha = 4\pi k/\lambda$, near its absorption edge,[9] where λ is the photon wavelength and k is the extinction coefficient. The values of k can be calculated from measured pseudo-dielectric function $\langle\varepsilon\rangle = \varepsilon_1 + i\varepsilon_2$ by the complex relation $(n + ik)^2 = (\varepsilon_1 + i\varepsilon_2)$ with n being the index of refraction. We employ the most commonly used Tauc plot method to acquire E_g.[9] Tauc *et al.* have shown the expression $[n(E)\alpha(E)E]^{1/2}$ varies linearly with $(E-E_g)$ near the absorption edge of some amorphous materials. Fig. 1 shows the typical extraction of optical bandgap of Al_2O_3 with

a)E-mail: nhan.nguyen@nist.gov. Telephone: (301) 975 2044. Fax: (301) 975 8069.

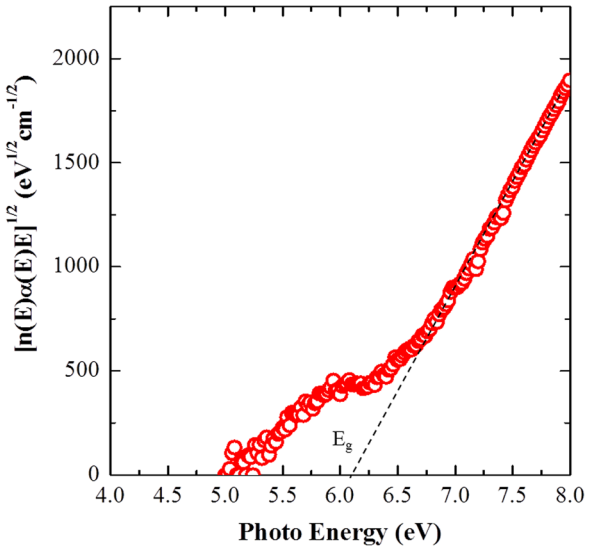

FIG. 1. Determination of Al_2O_3 band gap from the Tauc-plot by linear fitting of $[n(E)\alpha(E)E]^{1/2}$ where n(E) is the index of refraction and $\alpha(E)$ is the absorption coefficient.

the Tauc plot method. The non-linear plateau from 5 to 6 eV is likely due to the sub-bandgap defects in the oxide.[10] The optical band gap E_g of Al_2O_3 and HfO_2 are listed in Table I.[11] PDA of Al_2O_3 film yields a slightly improved gate oxide corresponding to the rise in band gap and minor increase in the index of refraction.

In this study, an IPE system consisting of a 150 Watt broadband Xenon light source is used in conjunction with a grating monochromator to provide a spectral range from 1.5 to 5.5 eV. Two long pass filters are used to filter out higher order dispersions. Light from the monochromator is collimated by a UV-grade achromatic lens and focused down on to the metal electrode surface of a MOS device by another UV grade achromatic lens to form a millimeter size spot. The position of the focal point on the surface of the device is automatically adjusted by moving the second lens according to the wavelength. A regulated power supply provides the bias applied to the MOS capacitor. An electrometer with sub-pico-ampere precision records the current while the monochromator scans the spectral range. The quantum yield Y is obtained by expression

$$I = PY/hv, \tag{1}$$

TABLE I. Summary of oxide band gap E_g, photoemission threshold of InP VB to Al_2O_3 and HfO_2 CB Φ_{semi}, and threshold for photoemission from Al to Al_2O_3.

Gate Oxide	Sample	E_g (eV)	Φ_{semi} (eV)	Φ_{Al} (eV)
Al_2O_3	n-type (100)	6.17	…	…
	n-type (100) PDA	6.31	3.44	2.70
	n-type (111)	6.11	3.37	2.79
	n-type (111) PDA	6.19	3.47	2.43
	p-type (111)	6.18	3.50	2.92
	p-type (111) PDA	6.26	3.53	2.31
HfO_2	SI(100) PDA	5.83	3.89	…
	SI(100) Passivated, PDA	…	3.95	…

where I is the measured current in amperes, P is the absorbed light power in watts, and hv is the photon energy in electron-volts.[12] The measured currents are corrected for stray light and possible tunneling and background noise. By using SE, we measured the complex indices of refraction and the thickness of each layer in the MOS structure. This information is necessary to be able to correct the incident light flux for attenuations and reflections in the MOS stack using a transfer-matrix method.[13] Carriers with minimum barrier energy (Φ) at the interface, once transferred to the collector (i.e., insulator layer), produce a yield

$$Y(hv) = A(hv)[hv - \Phi]^p, \tag{2}$$

where p depends on the energy distribution of photo-excited carriers at the interface. For semiconductor/insulator and metal/insulator interfaces with excitation photon energy near and above Φ, $p = 3$ and 2, respectively.[14,15] The cube root or the square root (depending on the origins of photoemission) of the yield is usually plotted vs. photon energy. The linear regions are then fitted, and the thresholds can be extrapolated from the fitting of the measured $Y^{1/3}$ and $Y^{1/2}$. Through this method, we can directly obtain the field dependent barrier height at the semiconductor/insulator interface and metal/insulator interface.

For low and moderately doped semiconductors, the barrier heights can also be influenced by strength of the electric field at the interface due to image-force (Schottky effect).[15] The field-induced lowering of the barrier height is shown as

$$\Phi(F) = \Phi_0 - \int_0^x F(z)dz - \frac{q^2}{8\pi\varepsilon_0\varepsilon_i}, \tag{3}$$

where Φ_0 is zero field barrier height and F is the electric field.[16] The second term in Eq. (3) includes the contributions of the work function difference between the electrode and the semiconductor, the semiconductor surface potential, and the fix charge field.[16] When the fix charge is zero, the expression becomes

$$\Phi(F) = \Phi_0 - q\sqrt{\frac{qF}{4\pi\varepsilon_0\varepsilon_i}}, \tag{4}$$

with the distance between the emitter surface and the barrier top $x_m = \sqrt{q/(16\pi\varepsilon_0\varepsilon_i F)}$.

Thus, the field dependent barrier heights are again plotted in a Schottky plot. The zero-field barrier height is then established by a linear fitting of Φ vs. $F^{1/2}$ and extrapolation to zero-field ($F = 0$).

For a MOS structure, the barrier heights are shown schematically in the energy band diagram in Fig. 2. IPE measurements are performed in the spectral range from 1.5 to 5.5 eV with discrete increment of 0.05 eV. Bias voltages from −2 to 2 V in steps of 0.1 V are applied to the substrate. The effective electric field in the oxide layer is defined as the applied voltage minus the built-in potential V_{bi} that is determined at the applied voltage when the photocurrent switched direction near photoemission threshold.[17] PDA was observed to shift

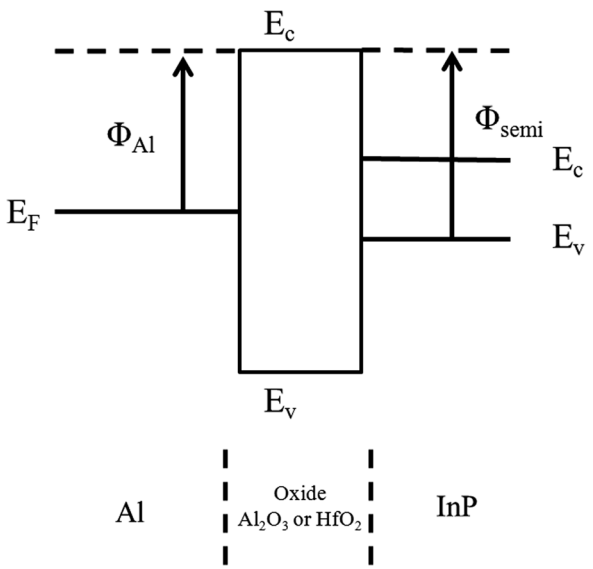

FIG. 2. Energy band diagram of Al/Oxide/InP MOS structure and barrier heights, Φ_{Al} for Al/oxide and Φ_{seni} oxide/InP interfaces (not drawn to scale).

the build-in potential up by a little over 0.1 V. There is no observable distinction in V_{bi} between the two crystal orientations (InP (100) versus (111)A). Oxide E_g of all samples are listed in Table I.

III. Al/Al_2O_3/InP

Fig. 3(a) shows the imaginary part $\langle \varepsilon_2 \rangle$ of the pseudodielectric function of InP obtained from SE measurement. There are four critical points, $E_0 = 3.15$ eV, $E_0 + \Delta_0 = 3.27$ eV, $E_0' = 4.7$ eV, and $E_0' + \Delta_0' = 4.93$ eV.[18] Plateau regions on the IPE yield $Y^{1/3}$ (Fig. 3(b)) showing the reduction in photocurrent coincide with the critical points at 3.15 and 4.7 eV. The reduction in photocurrent at E_0 and E_0' is due to direct optical transition between high symmetry points in the Brillouin zone of InP.[18,19] By comparing Figs. 3(a) and 3(b), the coincident features of the IPE yield and the SE spectra of InP become the clear indication of the photoemission originated from the InP substrate. These results demonstrate the use of SE as a powerful tool to supplement and verify data for an effective IPE measurement.

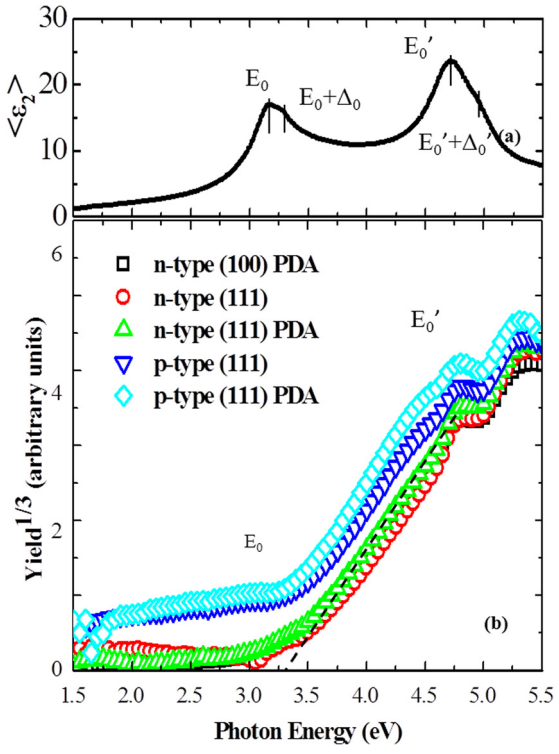

FIG. 3. (a) Imaginary part $\langle \varepsilon_2 \rangle$ of the pseudodielectric function of InP with four critical points; (b) cube root of the IPE yield as a function of photon energy for PDA and as-deposited Al_2O_3. All the IPE data shown were taken with the substrate biased at −2.0 V.

All $Y^{1/3}$ data measured at −2.0 V are plotted against photon energy in Fig. 3(b), which is representative of IPE of electrons from InP. We have discussed the choice of exponent p in Eq. (2) earlier. For the photoemission from a semiconductor, $p = 3$ is conventionally followed, and thus $Y^{1/3}$ is plotted vs. photon energy. In the region below threshold, higher yield is observed for the p-type sample. This observation is due to the higher background noise associated with measurements on particular samples with high gate leakage current. To extract the electric field depending threshold, we fit (dashed line) the linear region of data. Fig. 3(b) only shows the $Y^{1/3}$ at −2 V for simplicity. The fitting yields the energy threshold between the top of the VB of InP and the bottom of the CB of Al_2O_3. By fitting each individual bias, we can obtain the spectral thresholds at various electric field strengths in the oxide layer and plot them in the Schottky coordinates as shown in Fig. 4.

As we have discussed before, the energy thresholds are dependent of the applied electric field due to image-force lowering of the barrier.[16] Therefore, by linear-fitting the thresholds, Φ_{semi}, the barrier height between the valence band of semiconductor and the conduction band of the oxide at zero fields can be obtained, which are listed in Fig. 4. Nonlinear drop of barrier height is observed at field strengths beyond 1.25 $MV^{1/2}/cm^{1/2}$. This is due to high field

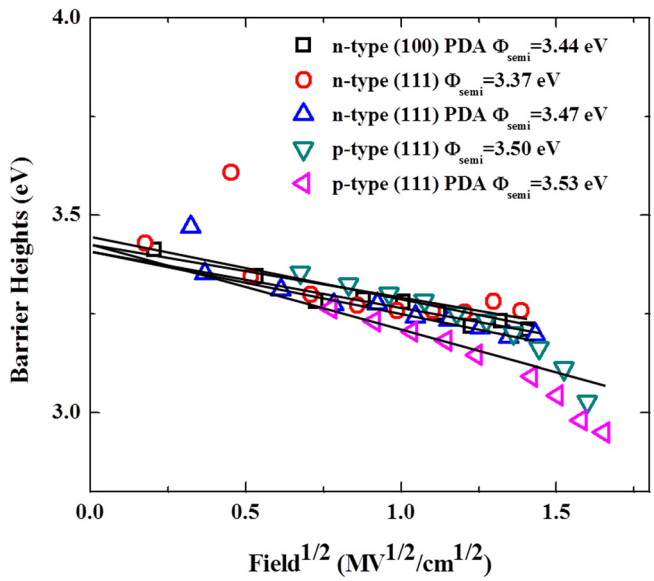

FIG. 4. Schottky plots showing field dependence of the barrier height for PDA and as-deposited samples and the zero field barrier heights for photoemission from VB of InP to CB of Al_2O_3.

penetration, which causes the barrier height to deviate from the ideal image-force lowering model and to lose its linearity.[7] Close examination of Fig. 4 shows annealing shifts the threshold upwards, and p-type material exhibits slightly higher Φ_{semi}. The (111)A crystal orientation of InP has a barrier that is about 0.03 eV less than that of the (100) surface. The effect on the threshold energy is minimal, despite the observation of significantly increased device performance by switching from (100) to (111) direction on InP and GaAs reported by Xu *et al.*[20]

An interlayer oxide was suggested in the previous report by Chou, *et al.*,[8] based on the observation of the tailing off of IPE yield curve below threshold. In addition to the TEM result, the interlayer was identified by the nonlinear regions of the sub-threshold yield, because of the extra steps required for the excited carriers to take from the InP substrate over the interlayer and to the conduction band of the oxide. However, our data exhibit well defined linearity from the onset of emission to 4.5 eV, which signifies the direct transition of carriers from the valence band of InP to the conduction band of Al_2O_3. There is no sub-threshold feature indicating such interlayer between the InP substrate and Al_2O_3 from this investigation. This means a cleaner InP/Al_2O_3 interface comparing with the earlier IPE measurement report. The difference of interface qualities could be due to the BOE/$(NH_4)_2$ S pre-deposition surface treatment explored in this work, vs. the HCl/$(NH_4)_2$ S or UV/O_3 treatment, as described in Chou, *et al.*'s report.[8] Recent XPS studies of the ALD high-κ growth InP have also shown reduced interfacial oxide formation at the interface with various Sulfur-based pre-deposition passivation treatments.[21]

To get the barrier height between Al and Al_2O_3, we plot $Y^{1/2}$-$h\nu$ and use a linear fit, as shown in Fig. 5(a), for the case of 2.0 V bias. Again, we consider the choice of exponent p in Eq. (2). Classically, for the photoemission from the Fermi level of a metallic material to the conduction band of the oxide, the yield is proportional to the square of the barrier height, and thus the square root of the yield is plotted against photon energy. Similar to Φ_{semi}, the zero field metal-oxide thresholds, denoted by Φ_{Al}, are extracted by linear fitting of the field-dependent barrier height plotted in the Schottky plot in Fig. 5(b). Ideally, Φ_{Al} should be independent of the semiconductor substrate material, which is consistent with the measurement result as the distinctions of threshold energy between various substrates are minimal. However, the annealing affects the threshold by shifting the barrier downwards. The variation of barrier height of same annealing condition is likely the result of exposure to air prior to gate metallization, since it is known that the Al/Al_2O_3 interface is sensitive to its chemical nature.[21]

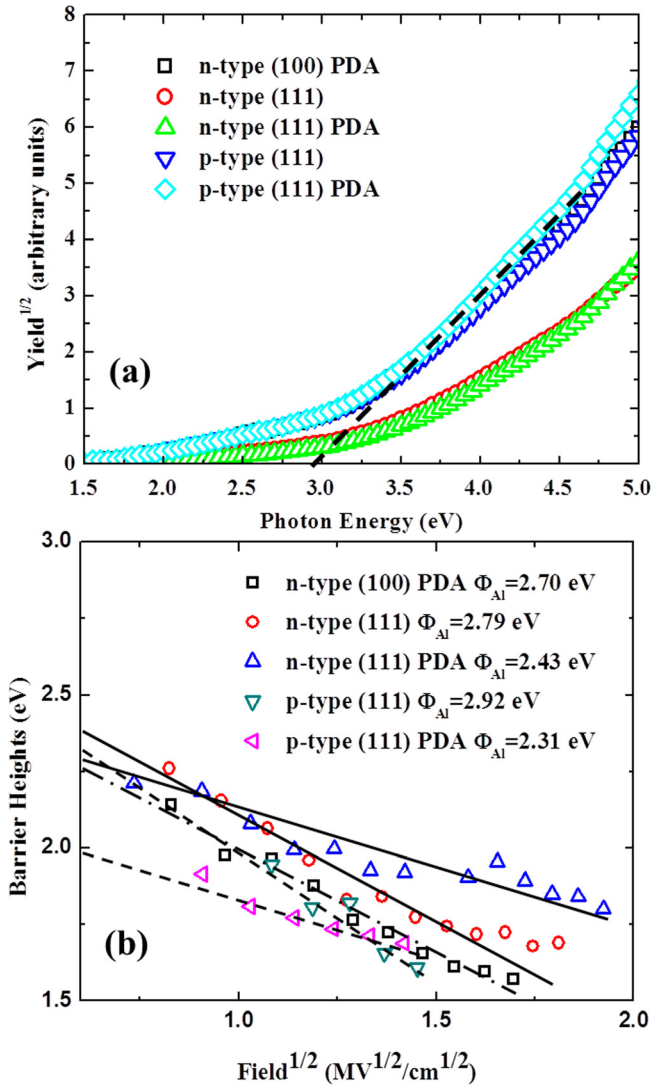

FIG. 5. (a) Typical Powell plots of Al/Al_2O_3 for PDA and as-deposited samples. All the IPE data shown were taken with the substrate biased at + 2.0 V; (b) The Schottky plots show field dependence of the barrier heights and the zero-field thresholds.

IV. Al/HfO_2/InP

Presented in Fig. 6 is the cube root of the yield data of the injection of elections from the InP valence band to the conduction band of HfO_2, plotted against photon energy. Again, we correlate the photoemission yield in Fig. 6 to the pseudo-dielectric function measured by SE in Fig. 3(a). Reduced photoelectron yield at 4.7 eV correspond to E_0'

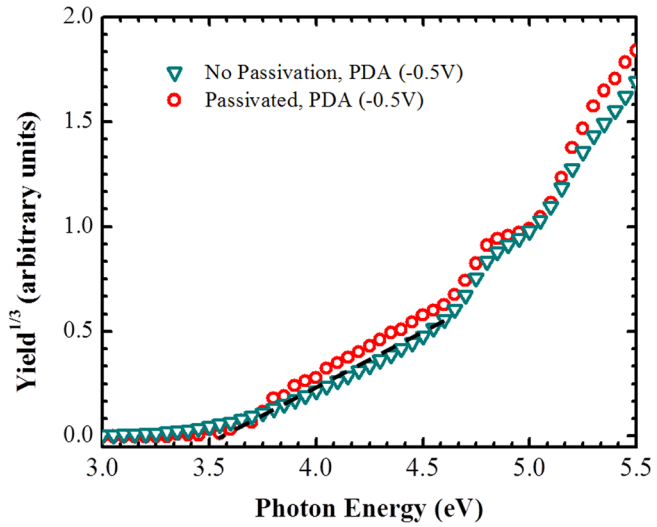

FIG. 6. Cube root of the IPE yield as a function of photon energy for electron injection from InP to HfO_2.

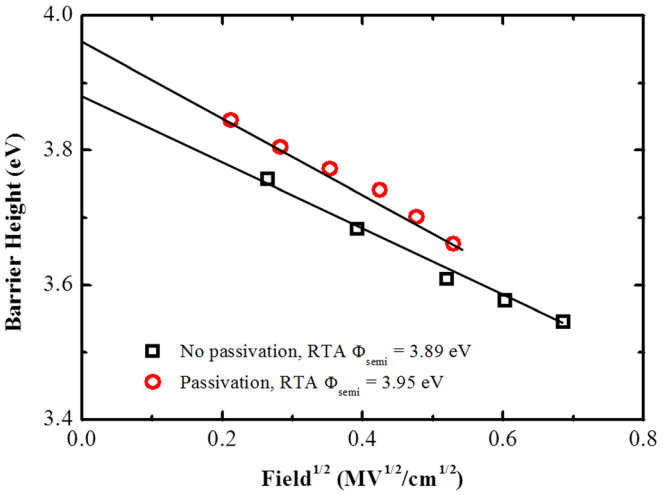

FIG. 7. Schottky plots showing field dependence of the barrier height and the zero field barrier heights for photoemission from VB of InP to CB of HfO_2.

signature of InP, seen in curves in both process conditions. $Y^{1/3}$ increases linearly with photon energy near the threshold. By fitting linearly to $Y^{1/3}$, we are able to obtain the threshold for the onset of electron injection from the InP VB top to the HfO_2 CB bottom. Similarly, the thresholds are determined for each bias and plotted in Fig. 7, from which we extracted the zero-field barrier height at the HfO_2/InP interface. Without $(NH_4)_2S$ surface passivation, the barrier height was found to be 3.89 eV. The passivated interface gains an increase of 60 meV in barrier height. The results suggest that the passivation suppresses energy levels close to the valence band edge inside the InP band gap. As with the Al_2O_3/InP case, there is no evidence showing any interface layer between HfO_2 and the InP substrate from the IPE measurement results.

V. CONCLUSIONS

In summary, IPE and SE are used to study the band offsets of ALD Al_2O_3 on n- and p-type InP with (100) and (111)A orientations under different post-deposition annealing conditions. Excellent linearity of the IPE yield is observed indicating good interface quality with low recombination rate, and the interlayer reported in past literatures is not evident in our experiments. The semiconductor-oxide barrier height of (111)A is 0.03 eV higher than that of (100) orientation. 500 °C PDA reduces the semiconductor-oxide threshold but increases the metal-oxide threshold. The barrier height at HfO_2/InP interface is also measured by IPE to be 3.89 eV for the sample without passivation treatment and 3.95 eV when the oxide-semiconductor interface is passivated. The barrier height of around 3.5 eV for the Al_2O_3/InP interface and around 3.9 eV for the HfO_2/InP interface demonstrates sufficiently large band offsets for the design of high performance MOSFET devices.

[1]S. Sze, *Semiconductors Devices, Physics and Technology* (Wiley, NY, 2003), p. 537.
[2]Y. Q. Wu, Y. Xuan, T. Shen, P. D. Ye, Z. Cheng, and A. Lochtefeld, Appl. Phys. Lett. **91**, 022108 (2007).
[3]Y. Wang, Y.-T. Chen, H. Zhao, F. Xue, F. Zhou, and J. C. Lee, Appl. Phys. Lett. **98**, 043506 (2011).
[4]H. Zhao, D. Shahrjerdi, F. Zhu, H.-S. Kim, I. Ok, M. Zhang, J. H. Yum, S. K. Banerjee, and J. C. Lee, Electrochem. Solid-State Lett. **11**, H233 (2008).
[5]C. Wang, M. Xu, R. Colby, D. W. Zhang, and P. D. Ye, Electrochem. Solid-State Lett. **15**(2), H27–H30 (2012).
[6]M. Xu, J. J. Gu, C. Wang, D. M. Zhernokletov, R. M. Wallace, and P. D. Ye, "New Insights in the Passivation of High-k/InP through Interface Characterization and MOSFET Demonstration: Impact of Crystal Orientation," IEEE Trans. Electron Devices (submitted).
[7]V. V. Afanas'ev, *Internal Photoemission Spectroscopy: Principles and Applications* (Elsevier, Amsterdam, 2008).
[8]H.-Y. Chou, V. V. Afanas'ev, A. Stesmans, H. C. Lin, P. K. Hurley, and S. B. Newcomb, Appl. Phys. Lett. **97**, 132112 (2010).
[9]J. Tauc, R. Grigorovici, and A. Vancu, Phys. Status Solidi **15**, 627 (1966).
[10]D. H. Hill, R. A. Bartynski, N. V. Nguyen, A. C. Davydov, D. Chandler-Horowitz, and M. M. Frank, J. Appl. Phys. **103**, 093712 (2008).
[11]N. V. Nguyen, S. Sayan, I. Levin, J. R. Ehrstein, I. J. R. Baumvol, C. Driemeier, C. Krug, L. Wielunski, P. Y. Hung, and A. Diebold, J. Vac. Sci. Technol. A **23**, 1706–1713 (2005).
[12]N. V. Nguyen, O. A. Kirillov, and J. S. Suehle, Thin Solid Films **519**(9), 2811–2816 (2011).
[13]S. J. Orfanidis, *Electromagnetic Waves and Antennas* (2010). Available at: http://www.ece.rutgers.edu/~orfanidi/ewa/.
[14]R. H. Fowler, Phys. Rev. **38**(1), 45–56 (1931).
[15]R. J. Powell, J. Appl. Phys. **41**, 2424 (1970).
[16]S. M. Sze, *Physics of Semiconductor Devices* (Wiley, 1981).
[17]N. V. Nguyen, M. Xu, O. A. Kirillov, P. D. Ye, C. Wang, K. Cheung, and J. S. Suehle, Appl. Phys. Lett. **96**, 052107 (2010).
[18]C. M. Herzinger, P. G. Snyder, B. Johs, and J. A. Woollam, J. Appl. Phys. **77**, 1715 (1995).
[19]D. E. Aspnes and A. A. Studna, Phys. Rev. B **27**, 985 (1983).
[20]M. Xu, K. Xu, R. Contreras, M. Milojevic, T. Shen, O. Koybasi, Y. Q. Wu, R. M. Wallace, and P. D. Ye, in 2009 *IEEE International Electron Devices Meeting (IEDM)* (Baltimore, MD, USA, 2009), pp. 1–4; V. V. Afanas'ev and A. Stesmans, J. Appl. Phys. **102**, 081301 (2007).
[21]B. Brennan, H. Dong, D. Zhernokletov, J. Kim, and R. M. Wallace, Appl. Phys. Express **4**, 125701 (2011).